Efficient simulation of multidimensional phonon transport using energy-based variance-reduced Monte Carlo formulations

Jean-Philippe M. Péraud and Nicolas G. Hadjiconstantinou
Department of Mechanical Engineering, Massachusetts Institute of Technology, Cambridge, Massachusetts 02139, USA
(Received 13 August 2011; published 21 November 2011)

We present a Monte Carlo method for obtaining solutions of the Boltzmann equation to describe phonon transport in micro- and nanoscale devices. The proposed method can resolve arbitrarily small signals (e.g., temperature differences) at small constant cost and thus represents a considerable improvement compared to traditional Monte Carlo methods, whose cost increases quadratically with decreasing signal. This is achieved via a control-variate variance-reduction formulation in which the stochastic particle description solves only for the deviation from a nearby equilibrium, while the latter is described analytically. We also show that simulation of an energy-based Boltzmann equation results in an algorithm that lends itself naturally to exact energy conservation, thereby considerably improving the simulation fidelity. Simulations using the proposed method are used to investigate the effect of porosity on the effective thermal conductivity of silicon. We also present simulations of a recently developed thermal conductivity spectroscopy process. The latter simulations demonstrate how the computational gains introduced by the proposed method enable the simulation of otherwise intractable multiscale phenomena.

DOI: 10.1103/PhysRevB.84.205331 PACS number(s): 63.20.−e

I. INTRODUCTION

Over the past two decades, the dramatic advances associated with microelectromechanical systems (MEMS) and nanoelectromechanical systems (NEMS) have attracted significant attention to microscale and nanoscale heat transfer considerations.[1] Applications range from thermal management of electronic devices[2] to the development of thermoelectric materials with higher figures of merit.[3] The thermoelectric figure of merit is proportional to the electrical conductivity and inversely proportional to the thermal conductivity and can thus be improved by reducing the latter and/or increasing the former. One of the most promising approaches toward reducing the thermal conductivity of thermoelectric materials is the introduction of nanostructures that interact with the ballistic motion of phonons at small scales, thus influencing heat transport.[4] Such an approach requires a reliable description of phonon transport at the nanoscale and cannot rely on Fourier's law, which is valid for diffuse transport. On the other hand, first-principles calculations (e.g., molecular dynamics approaches, classical or quantum mechanical) are too expensive for treating phonon transport at the device (e.g., micrometer) scale. At these scales, a kinetic description based on the Boltzmann transport equation (BTE) offers a reasonable balance between fidelity and model complexity and is able to accurately describe the transition from diffusive to ballistic transport as characteristic system length scales approach and ultimately become smaller than the phonon mean free path.

Solution of the BTE is a challenging task, especially in complex geometries. The high dimensionality of the distribution function coupled with the ability of particle methods to naturally simulate advection processes without stability problems[5] make particle Monte Carlo methods particularly appealing. Following the development of the direct Monte Carlo method by Bird[6] for treating dilute gases, Monte Carlo methods for phonon transport were first introduced by Peterson[7] and subsequently improved by Mazumder and Majumdar.[8] Over the past decade, further important refinements have been introduced: Lacroix *et al*. introduced a method to treat frequency-dependent mean free paths;[9] Jeng *et al*. introduced a method for efficiently treating transmission and reflection of phonons at material interfaces and used this method to model the thermal conductivity of nanoparticle composites;[4] Hao *et al*. developed[10] a formulation for periodic boundary conditions in order to study the thermal conductivity of periodic nanoporous materials while simulating only one unit cell (period).

The work presented here introduces a number of improvements which enable efficient and accurate simulation of the most challenging phonon transport problems, namely, three dimensional and transient. Accuracy is improved compared to previous approaches by introducing an energy-based formulation, which simulates energy packets rather than phonons; this formulation makes energy conservation particularly easy to implement rigorously, in contrast to previous approaches which were *ad hoc* and in many cases ineffective. We also introduce a variance-reduced formulation for substantially reducing the statistical uncertainty associated with sampling solution (temperature and heat flux) fields. This formulation is based on the concept of control variates, first introduced in the context of Monte Carlo solutions of the Boltzmann equation for dilute gases;[5] it relies on the fact that signal strength is intimately linked to deviation from equilibrium, or, in other words, that the large computational cost associated with small signals is due to the fact that in these problems the deviation from equilibrium is small. This observation can be exploited by utilizing the nearby equilibrium state as a "control" and using the Monte Carlo method to calculate the contribution of nonequilibrium therefrom. Because the deviation from equilibrium is small, only a small quantity is evaluated stochastically (the fields associated with the equilibrium component are known analytically), resulting in small statistical uncertainty; moreover, the latter decreases as

the deviation from equilibrium decreases, thus enabling the simulation of arbitrarily small deviations from equilibrium.

In the technique presented here, we use particles to simulate the deviation from equilibrium, and it is thus referred to as a deviational method; the origin of this methodology can be found in the low-variance deviational simulation Monte Carlo method[11–14] recently developed for dilute gases. The theoretical basis underlying this method as well as the modifications required for use in phonon transport simulations are described in Sec. II C. The resulting algorithm is described in Sec. III and validated in Sec. IV.

The proposed algorithm is used to obtain solutions to two problems of practical interest. The first application studies the thermal conductivity of porous silicon containing voids with different degrees of alignment and is intended to showcase how ballistic effects influence the "effective" thermal conductivity. The second application is related to the recently developed experimental method of "thermal conductivity spectroscopy"[15] based on the pump-probe technique known as transient thermoreflectance, which uses the response of a material to laser irradiation to infer information about physical properties of interest[16] (e.g., the mean free paths of the dominant heat carriers).

II. THEORETICAL BASIS

A. Summary of traditional Monte Carlo simulation methods

We consider the Boltzmann transport equation in the frequency-dependent relaxation-time approximation

$$\frac{\partial f}{\partial t} + \mathbf{V}_g(\omega,p)\nabla f = -\frac{f - f^{\mathrm{loc}}}{\tau(\omega,p,T)}, \tag{1}$$

where $f = f(t,\mathbf{x},\mathbf{k},p)$ is the phonon distribution function in phase space, $\omega = \omega(\mathbf{k},p)$ the phonon radial frequency, p the phonon polarization, and T the temperature; similarly to the nomenclature adopted in Ref. 1, f is defined in reference to the occupation number. For example, if the system is perfectly thermalized at temperature T, f is a Bose-Einstein distribution,

$$f_T^{eq} = \frac{1}{\exp\left(\frac{\hbar\omega(\mathbf{k},p)}{k_b T}\right) - 1}, \tag{2}$$

where k_b is Boltzmann's constant. Also, f^{loc} is an equilibrium (Bose-Einstein) distribution parametrized by the *local pseudotemperature* defined more precisely in Sec. II A 2.

In this work we consider longitudinal acoustic (LA), transverse acoustic (TA), longitudinal optical (LO), and transverse optical (TO) polarizations; acoustic phonons are known to be the most important contributors to lattice thermal conductivity.[17,18] The phonon radial frequency is given by the dispersion relation $\omega = \omega(\mathbf{k},p)$. Phonons travel at the group velocity $\mathbf{V}_g = \nabla_k\omega$.

In the following, we always consider the ideal case where the dispersion relation is isotropic. For convenience, the radial frequency ω and two polar angles θ and ϕ are usually preferred as primary parameters compared to the wave vector. Equation (1) is simulated using computational particles that represent phonon bundles, namely, collections of phonons with similar characteristics (the position vector $\mathbf{x}$, the wave vector $\mathbf{k}$, and the polarization or propagation mode p), using the approximation

$$\frac{1}{8\pi^3} f(t,\mathbf{x},\mathbf{k},p) \approx N_{\mathrm{eff}} \sum_i \delta^3(\mathbf{x}-\mathbf{x}_i)\delta^3(\mathbf{k}-\mathbf{k}_i)\delta_{p,p_i}, \tag{3}$$

where $\mathbf{x}_i$, $\mathbf{k}_i$, and p_i respectively represent the position, the wave vector, and the polarization of particle i and N_{eff} is the number of phonons in each phonon bundle. The factor $1/8\pi^3$ is necessary for converting the quantity representing the occupation number, f, into a quantity representing the phonon density in phase space. Written in polar coordinates, and using the frequency instead of the wave number, this expression becomes

$$\frac{D(\omega,p)}{4\pi} f(t,\mathbf{x},\omega,\theta,\phi,p)\sin(\theta) \approx N_{\mathrm{eff}} \sum_i \delta^3(\mathbf{x}-\mathbf{x}_i)\delta(\omega-\omega_i)\delta(\theta-\theta_i)\delta(\phi-\phi_i)\delta_{p,p_i}, \tag{4}$$

where ω_i, θ_i, and ϕ_i respectively represent the radial frequency, the polar angle, and the azimuthal angle of particle i. The density of states $D(\omega,p)$ is made necessary by the use of ω as a primary parameter and is given by

$$D(\omega,p) = \frac{k(\omega,p)^2}{2\pi^2 V_g(\omega,p)}. \tag{5}$$

1. Initialization

Systems are typically initialized in an equilibrium state at temperature T; the number of phonons in a given volume V is calculated using the Bose-Einstein statistics

$$N = V \int_{\omega=0}^{\omega_{\max}} \sum_p D(\omega,p) f_T^{eq}(\omega) d\omega, \tag{6}$$

where $\omega_{\max}$ is the maximum (cutoff) frequency and f_T^{eq} is the occupation number at equilibrium at temperature T.

The number of computational particles (each representing a phonon bundle) is given by N/N_{eff}. The value of N_{eff} is determined by balancing computational cost (including storage) with the need for a sufficiently large number of particles for statistically meaningful results.

2. Time integration

Once the system is initialized, the simulation proceeds by applying a splitting algorithm with time step Δt. Integration for one time step is comprised of three substeps:

(1) The advection substep, during which bundle i moves by $\mathbf{V}_{g,i}\Delta t$.

(2) The sampling substep, during which the temperature (T) and pseudotemperature (T_{loc}) are locally measured. They are calculated by inverting the local energy (E) and pseudoenergy ($\tilde{E}$)[10] relations,

$$E = N_{\mathrm{eff}} \sum_i \hbar\omega_i = V \int_{\omega=0}^{\omega_{\max}} \sum_p \frac{D(\omega,p)\hbar\omega}{\exp\left(\frac{\hbar\omega}{k_b T}\right) - 1} d\omega \tag{7}$$

and

$$\tilde{E} = N_{\text{eff}} \sum_i \frac{\hbar\omega_i}{\tau(\omega_i, p_i, T)} = V \int_{\omega=0}^{\omega_{\max}} \sum_p \frac{D(\omega,p)\hbar\omega}{\tau(\omega,p,T)} \frac{1}{\exp\left(\frac{\hbar\omega}{k_b T_{\text{loc}}}\right) - 1} d\omega, \quad (8)$$

respectively.

(3) The scattering substep, during which each phonon i is scattered according to its scattering probability given by

$$P_i = 1 - \exp\left(-\frac{\Delta t}{\tau(\omega_i, p_i, T)}\right). \quad (9)$$

Scattering proceeds by drawing new frequencies, polarizations, and traveling directions. Because of the frequency-dependent relaxation times, frequencies must be drawn from the distribution $D(\omega,p) f^{\text{loc}}/\tau(\omega,p,T)$. Since scattering events conserve energy, the latter must be conserved during this substep. However, because the frequencies of the scattered phonons are drawn randomly, conservation of energy is enforced by adding or deleting particles until a target energy is approximately reached.[8,9] In addition to being approximate, this method does not always ensure that energy is conserved, resulting in random walks in the energy of the simulated system, which in some cases leads to deterministic error. In the next section, we present a convenient way for rigorously conserving energy.

B. Energy-based formulation

While most computational techniques developed so far conserve energy in only an approximate manner,[8,9] here we show that an energy-based formulation provides a convenient and rigorous way to conserve energy in the relaxation time approximation.

Adopting a similar approach as in Ref. 2 to derive the *equation of phonon radiative transfer*, we multiply (1) by $\hbar\omega$ to obtain

$$\frac{\partial e}{\partial t} + \mathbf{V}_g \nabla e = \frac{e^{\text{loc}} - e}{\tau}, \quad (10)$$

which we will refer to as the energy-based BTE. Here, $e = \hbar\omega f$ and $e^{\text{loc}} = \hbar\omega f^{\text{loc}}$. Equation (10) can be simulated by writing

$$e \approx 8\pi^3 \mathcal{E}_{\text{eff}} \sum_i \delta^3(\mathbf{x} - \mathbf{x}_i)\delta^3(\mathbf{k} - \mathbf{k}_i)\delta_{p,p_i}, \quad (11)$$

where $\mathcal{E}_{\text{eff}}$ is defined as the effective energy carried by each computational particle. Statement (11) defines computational particles that all represent the same amount of energy. From the point of view of phonons, comparison of (3) and (11) shows that the effective number of phonons represented by the newly defined particles is variable and is linked to the effective energy by the relation $\mathcal{E}_{\text{eff}} = N_{\text{eff}}\hbar\omega$. By analogy with the description of Sec. II A, computational particles defined by (11) obey the same computational rules as in the previous Monte Carlo approaches. Modifications appear at three levels:

(1) When drawing particle frequencies during initialization, emission from boundaries, or scattering, the distribution functions that we use must account for the factor $\hbar\omega$. For example, when initializing an equilibrium population of particles at a temperature T, one has to draw the frequencies from the distribution

$$\frac{\hbar\omega \sum_p D(\omega,p)}{\exp\left(\frac{\hbar\omega}{k_b T}\right) - 1}. \quad (12)$$

(2) Calculation of the energy in a cell is straightforward and simply consists in counting the number of computational particles. The energy associated with N particles is given by $\mathcal{E}_{\text{eff}} N$.

(3) Since the energy in a cell is proportional to the number of particles, there is no need for an addition or deletion process: *energy is strictly and automatically conserved by simply conserving the number of particles*.

C. Deviational formulation

In this section we introduce an additional modification which dramatically decreases the statistical uncertainty associated with Monte Carlo simulations of (10). Our approach belongs to a more general class of control-variate variance-reduction methods for solving kinetic equations,[5,11,19] in which the moments $\langle R \rangle$ of a given distribution f are computed by writing

$$\int R f \, d\mathbf{x} d\mathbf{c} = \int R(f - f^{eq}) d\mathbf{x} d\mathbf{c} + \int R f^{eq} d\mathbf{x} d\mathbf{c}, \quad (13)$$

where the first term of the right-hand side is computed stochastically and the second term is computed deterministically. If $f^{eq} \approx f$, the variance reduction is large because only a small term is determined stochastically (see Figs. 1 and 2).

In the present context, this methodology provides significant computational savings when an equilibrium (constant-temperature) state exists nearby, which is precisely the regime in which statistical noise becomes problematic (low signals). The degree of variance reduction achieved by this method is quantified in Sec. V.

Let

$$e^{eq}_{T_{eq}}(\omega) = \frac{\hbar\omega}{\exp\left(\frac{\hbar\omega}{k_b T_{eq}}\right) - 1}, \quad (14)$$

where $T_{eq} \neq T_{eq}(\mathbf{x},t)$. Then, it is straightforward to show that $e^d = e - e^{eq}_{T_{eq}}$ is governed by

$$\frac{\partial e^d}{\partial t} + \mathbf{V}_g \nabla e^d = \frac{\left(e^{\text{loc}} - e^{eq}_{T_{eq}}\right) - e^d}{\tau}. \quad (15)$$

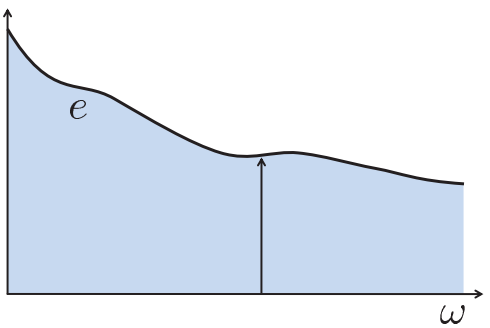

FIG. 1. (Color online) In standard particle methods, the moments of the distribution are stochastically integrated.

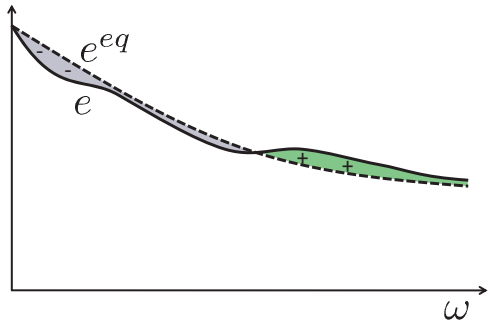

FIG. 2. (Color online) In a control-variate formulation, the stochastic part is reduced to the calculation of the deviation from a known state, which is much smaller.

Therefore, by analogy to the standard particle methods for solving the Boltzmann equation, we define computational particles by

$$e^d = e - e^{eq}_{T_{eq}} \approx 8\pi^3 \mathcal{E}^d_{\text{eff}} \sum_i s(i)\delta^3(\mathbf{x}-\mathbf{x}_i)\delta^3(\mathbf{k}-\mathbf{k}_i)\delta_{p,p_i}, \quad s(i) = \pm 1. \tag{16}$$

We will refer to these newly defined computational particles as deviational particles. Clearly, deviational particles may be negative since $e - e^{eq}_{T_{eq}}$ can be a negative quantity. This is accounted for by the sign term in Eq. (16). In what follows, we derive evolution rules for deviational particles based on (15).

III. ALGORITHM

The variance-reduced algorithm is very similar to its non-variance-reduced counterpart and comprises an initialization step followed by a splitting algorithm for time integration. The main change lies in the distributions from which deviational particles are sampled.

A. Initialization

The algorithm proceeds by choosing the equilibrium state at temperature T_{eq} from which deviations will be simulated. Although this choice can be quite critical in the efficiency of the method (the smaller the deviation from the chosen equilibrium state, the smaller the number of deviational particles required for a given statistical uncertainty, or, for a fixed number of deviational particles, the larger the variance reduction), it is usually a natural and intuitive choice.

In some cases, the equilibrium state is the same as the initial state. In such a situation, the simulation starts with no particles. Nevertheless, one still has to choose the deviational effective energy $\mathcal{E}^d_{\text{eff}}$ for subsequent use. In the various examples discussed below, this parameter was chosen as follows: Based on a guess of the upper bound on the deviation of temperature at steady state, the deviational energy of the system can be estimated using

$$\Delta E = \int_{\omega=0}^{\omega_{\max}} \sum_p \hbar\omega D(\omega,p) \times \left| \frac{1}{\exp\left(\frac{\hbar\omega}{k_b T}\right)-1} - \frac{1}{\exp\left(\frac{\hbar\omega}{k_b T_{eq}}\right)-1} \right| d\omega. \tag{17}$$

This estimate of the deviational energy allows $\mathcal{E}^d_{\text{eff}}$ to be (approximately) determined based on the desired number of computational particles.

If the initial state f^0 is different from the equilibrium distribution, particles need to be initialized in the computational domain. Their frequencies and polarizations are drawn from the distribution

$$D(\omega,p)e^d(\omega) = \hbar\omega D(\omega,p)\left[f^0 - \frac{1}{\exp\left(\frac{\hbar\omega}{k_b T_{eq}}\right)-1} \right]. \tag{18}$$

Typically, f^0 is an equilibrium distribution at some temperature T, whereby the above expression reduces to

$$D(\omega,p)e^d(\omega) = \hbar\omega D(\omega,p)\left[\frac{1}{\exp\left(\frac{\hbar\omega}{k_b T}\right)-1} - \frac{1}{\exp\left(\frac{\hbar\omega}{k_b T_{eq}}\right)-1} \right]. \tag{19}$$

This function is positive if $T > T_{eq}$ and negative if $T < T_{eq}$. As a result, in the latter case, particles are assigned a negative sign. Drawing of the frequencies is performed as in Ref. 8, namely, by subdividing the frequency range into bins (generally, about 1000 bins are considered enough), defining a discretized and normalized cumulative distribution from (19), uniformly drawing a random number between 0 and 1, and finding the bins to which it corresponds in order to match the normalized cumulative distribution.

B. Advection

Since the left-hand side of (15) is analogous to that of (1), the advection substep is unchanged. In other words, during the time step Δt, particles of group velocity $\mathbf{V}_g(\omega,p)$ are simply advected by $\mathbf{V}_g(\omega,p)\Delta t$.

C. Sampling substep

Sampling of the local temperature and pseudotemperature requires a few changes from the non-variance-reduced method, namely:

(1) Let C_j be the set of indices corresponding to the particles inside cell j of volume V_j at time t. Since each particle represents the same amount of energy, the deviational energy is given by

$$\Delta E_j = \mathcal{E}^d_{\text{eff}} \sum_{i\in C_j} s(i) = \mathcal{E}^d_{\text{eff}}(\mathcal{N}^+_j - \mathcal{N}^-_j), \tag{20}$$

where $\mathcal{N}^+_j$ and $\mathcal{N}^-_j$ are respectively the numbers of positive and negative particles inside the cell j.

(2) The corresponding temperature T_j is then calculated by numerically inverting the expression

$$\frac{\Delta E_j}{V_j} = \int_{\omega=0}^{\omega_{\max}} \sum_p D(\omega,p)\hbar\omega \times \left[\frac{1}{\exp\left(\frac{\hbar\omega}{k_b T_j}\right)-1} - \frac{1}{\exp\left(\frac{\hbar\omega}{k_b T_{eq}}\right)-1}\right] d\omega. \quad (21)$$

(3) Similarly, once T_j is known, the deviational pseudoenergy is computed using

$$\Delta\tilde{E}_j = \mathcal{E}^d_{\text{eff}} \sum_{i\in C_j} \frac{s(i)}{\tau(\omega_i,p_i,T_j)}. \quad (22)$$

(4) The corresponding pseudotemperature $[T_{\text{loc}}]_j$ is calculated by numerically inverting

$$\frac{\Delta\tilde{E}_j}{V_j} = \int_{\omega=0}^{\omega_{\max}} \sum_p \frac{D(\omega,p)\hbar\omega}{\tau(\omega,p,T_j)} \times \left[\frac{1}{\exp\left(\frac{\hbar\omega}{k_b [T_{\text{loc}}]_j}\right)-1} - \frac{1}{\exp\left(\frac{\hbar\omega}{k_b T_{eq}}\right)-1}\right] d\omega. \quad (23)$$

D. Scattering step

During the scattering step we integrate

$$\frac{de^d}{dt} = \frac{\left(e^{\text{loc}} - e^{eq}_{T_{eq}}\right) - e^d}{\tau(\omega,p,T_j)} \quad (24)$$

for a time step Δt, where

$$e^{\text{loc}} - e^{eq}_{T_{eq}} = \hbar\omega\left[\frac{1}{\exp\left(\frac{\hbar\omega}{k_b [T_{\text{loc}}]_j}\right)-1} - \frac{1}{\exp\left(\frac{\hbar\omega}{k_b T_{eq}}\right)-1}\right]. \quad (25)$$

We select the particles to be scattered according to the scattering probability (specific to each particle's frequency and polarization, and depending on the local temperature)

$$P(\omega_i,p_i,T_j) = 1 - \exp\left(-\frac{\Delta t}{\tau(\omega_i,p_i,T_j)}\right). \quad (26)$$

The pool of selected particles represents a certain amount of deviational energy $\mathcal{E}^d_{\text{eff}}(\mathcal{N}^+_{s,j} - \mathcal{N}^-_{s,j})$, where $\mathcal{N}^+_{s,j}$ and $\mathcal{N}^-_{s,j}$ refer respectively to the numbers of positive and negative selected (i.e., scattered) particles in cell j. This pool of selected particles must be replaced by particles with properties drawn from the distribution

$$\frac{D(\omega,p)\left(e^{\text{loc}} - e^{eq}_{T_{eq}}\right)}{\tau(\omega,p,T_j)} = \frac{D(\omega,p)\hbar\omega}{\tau(\omega,p,T_j)}\left(\frac{1}{\exp\left(\frac{\hbar\omega}{k_b [T_{\text{loc}}]_j}\right)-1} - \frac{1}{\exp\left(\frac{\hbar\omega}{k_b T_{eq}}\right)-1}\right), \quad (27)$$

which is either positive for all frequencies and polarizations or negative for all frequencies and polarizations. In other words, scattered particles must be replaced by particles which all have the same sign as $e^{\text{loc}} - e^{eq}_{T_{eq}}$ and which respect the energy conservation requirement. Therefore, out of the $\mathcal{N}^+_{s,j} + \mathcal{N}^-_{s,j}$ selected particles, we redraw properties for $|\mathcal{N}^+_{s,j} - \mathcal{N}^-_{s,j}|$ of them according to the distribution (27) and delete the other selected particles. The $|\mathcal{N}^+_{s,j} - \mathcal{N}^-_{s,j}|$ particles to be kept are chosen randomly inside the cell j and are given the sign of $e^{\text{loc}} - e^{eq}_{T_{eq}}$.

This process tends to reduce the number of particles in the system and counteracts sources of particle creation within the algorithm (e.g., see the boundary conditions discussed in the next section). A bounded number of particles is essential to the method stability, and the reduction process just described is a major contributor to the latter.[11,12] Hence, in a typical problem starting from an equilibrium state that is also chosen as the control, the number of particles will first increase from zero and, at steady state, reach a constant value that can be estimated by appropriate choice of $\mathcal{E}^d_{\text{eff}}$ as described in Sec. III A. The constant value will usually be higher than (but of the same order as) the estimated value: indeed, the rate of elimination of pairs of particles of opposite signs depends on the number of particles per cell and therefore on the spatial discretization chosen (the finer the discretization, the smaller the number of particles per cell and therefore the smaller the rate of elimination).

E. Boundary conditions

In phonon transport problems, various types of boundary condition appear. Isothermal boundary conditions, similar by nature to a blackbody, have been used in several studies.[8,9] Adiabatic boundaries also naturally appear.[8,20] Recently, a class of periodic boundary conditions has also been introduced.[10] The deviational formulation adapts remarkably well to these different classes of boundary conditions.

1. Adiabatic boundaries

Adiabatic boundaries reflect all incident phonons. This reflection process can be divided into two main categories: diffuse and specular reflection. In both cases, it is assumed that the polarization and frequency remain the same when a phonon is reflected. The only modified parameter during the process is the traveling direction.

(i) *Specular reflection* on a boundary ∂n of normal vector $\mathbf{n}$ can be expressed, in terms of the energy distribution, by

$$e(\mathbf{x},\mathbf{k}) = e(\mathbf{x},\mathbf{k}'), \quad (28)$$

where $\mathbf{k}' = \mathbf{k} - 2(\mathbf{k}\cdot\mathbf{n})\mathbf{n}$ and $\mathbf{x} \in \partial n$. Since the equilibrium distribution $e^{eq}_{T_{eq}}$ is isotropic, then substracting it from both sides simply yields

$$e^d(\mathbf{x},\mathbf{k}) = e^d(\mathbf{x},\mathbf{k}'). \quad (29)$$

In other words, deviational particles are specularly reflected.

(ii) *Diffuse reflection* amounts to randomization of the traveling direction of a phonon incident on the boundary, in order for the population of phonons leaving the boundary to be isotropic. Since an equilibrium distribution is already isotropic, incident deviational particles are treated identically to real phonons.

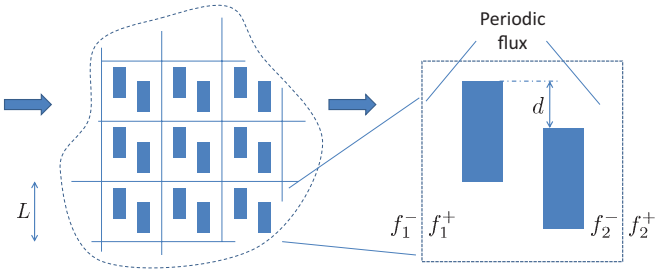

FIG. 3. (Color online) Example of a periodic nanostructure. Each periodic cell comprises two rectangular voids with diffusely reflecting walls. This nanostructure, and in particular the influence of the parameter d, is studied further in Sec. VI A.

2. Isothermal boundaries

In the case of an isothermal boundary at temperature T_b, incident phonons are absorbed, while the boundary itself, at temperature T_b, emits new phonons from the equilibrium distribution corresponding to T_b. The emitted heat flux per unit radial frequency is expressed by

$$q''_{\omega,b} = \frac{1}{4}\sum_p \frac{D(\omega,p)V_g(\omega,p)\hbar\omega}{\exp\left(\frac{\hbar\omega}{k_b T_b}\right)-1}. \tag{30}$$

Subtracting the heat flux per unit radial frequency corresponding to a boundary at equilibrium temperature, we obtain

$$q''_{\omega,b} = \frac{1}{4}\sum_p D(\omega,p)V_g(\omega,p)\hbar\omega \times \left(\frac{1}{\exp\left(\frac{\hbar\omega}{k_b T_b}\right)-1} - \frac{1}{\exp\left(\frac{\hbar\omega}{k_b T_{eq}}\right)-1}\right), \tag{31}$$

which gives the frequency distribution of emitted particles. Traveling directions must be chosen accordingly, as explained, for example, in Ref. 8.

3. Periodic unit cell boundary conditions

Heat transfer in periodic nanostructures is a subject of considerable interest in the context of many applications. Such nanostructures are considered by Hao *et al.*,[10] by Huang *et al.*,[21] and by Jeng *et al.*[4] Hao *et al.* developed periodic boundary conditions that allow efficient simulation of such structures by considering only one unit cell (period). In this section we review the work of Hao *et al.*[10] and explain how the deviational particle formulation presented here lends itself naturally to this type of boundary condition. Simulations using these boundary conditions are presented in Sec. VI A.

We consider the two-dimensional (2D) periodic structure depicted in Fig. 3, in which square unit cells containing two rectangular voids are organized in a square lattice. Our interest focuses on determining the effective thermal conductivity of such a structure as a function of d, the degree of alignment.

The formulation introduced by Hao *et al.* amounts to stating that, at the boundaries, the deviation of the phonon distribution from the local equilibrium is periodic. Using the notations from Fig. 3, this condition can be written as

$$\begin{aligned} f_1^+ - f_{T_1}^{eq} &= f_2^+ - f_{T_2}^{eq}, \\ f_1^- - f_{T_1}^{eq} &= f_2^- - f_{T_2}^{eq}, \end{aligned} \tag{32}$$

where $f_{T_1}^{eq}$ and $f_{T_2}^{eq}$ refer to the equilibrium distributions at temperatures T_1 and T_2, and the superscript $+$ denotes particles moving to the right (with respect to Fig. 3) and the superscript $-$ refers to particles moving to the left. This formulation enforces at the same time the periodicity of the heat flux and a temperature gradient. In terms of deviational energy distributions, this relation becomes

$$\begin{aligned} \hbar\omega\left(f_1^+ - f_{T_{eq}}^{eq} - f_{T_1}^{eq}\right) &= \hbar\omega\left(f_2^+ - f_{T_{eq}}^{eq} - f_{T_2}^{eq}\right), \\ \hbar\omega\left(f_1^- - f_{T_{eq}}^{eq} - f_{T_1}^{eq}\right) &= \hbar\omega\left(f_2^- - f_{T_{eq}}^{eq} - f_{T_2}^{eq}\right), \end{aligned} \tag{33}$$

which amounts to

$$\begin{aligned} e_1^{d,+} - e_{T_1}^{eq} &= e_2^{d,+} - e_{T_2}^{eq}, \\ e_1^{d,-} - e_{T_1}^{eq} &= e_2^{d,-} - e_{T_2}^{eq}. \end{aligned} \tag{34}$$

Computationally, this formulation can be implemented by emitting new particles from both sides while periodically advecting the existing particles. Without any loss of generality, let us assume that $T_1 > T_2$. Particles emitted from the hot side originate from the distribution

$$e_1^{d,+} = e_2^{d,+} + e_{T_1}^{eq} - e_{T_2}^{eq}. \tag{35}$$

Therefore, at a given point on the boundary, denoting by θ the angle with respect to the normal and by ϕ the azimuthal angle, the flux per unit radial frequency locally emitted from boundary 1 (the "hot" side) in the solid angle $d\Omega = \sin\theta d\theta d\phi$ can be expressed as

$$\begin{aligned} q''_{\omega,h} &= \sum_p e_1^{d,+}(\omega,\theta,\phi,p)\frac{D(\omega,p)}{4\pi}V_g(\omega,p)\cos\theta\sin\theta d\theta d\phi \\ &= \sum_p \underbrace{e_2^{d,+}\frac{D(\omega,p)}{4\pi}V_g(\omega,p)\cos\theta\sin\theta d\theta d\phi}_{\text{crossing boundary 2}} + \underbrace{\left(e_{T_1}^{eq} - e_{T_2}^{eq}\right)\frac{D(\omega,p)}{4\pi}V_g(\omega,p)\cos\theta\sin\theta d\theta d\phi}_{\text{new particles generated}}. \end{aligned} \tag{36}$$

Similarly, the flux per unit radial frequency locally emitted from boundary 2 (the "cold" boundary) can be expressed as

$$q''_{\omega,c} = \sum_p \underbrace{e_1^{d,-}\frac{D(\omega,p)}{4\pi}V_g(\omega,p)\cos\theta\sin\theta d\theta d\phi}_{\text{crossing boundary 1}} - \underbrace{\left(e_{T_1}^{eq} - e_{T_2}^{eq}\right)\frac{D(\omega,p)}{4\pi}V_g(\omega,p)\cos\theta\sin\theta d\theta d\phi}_{\text{new particles generated}}. \tag{37}$$

Hence the boundary condition can be enforced by the following:

(i) Moving all particles and applying periodic boundary conditions to those crossing a periodic boundary: a particle leaving the system on one side is reinserted on the other side.

(ii) Generating new particles from the distribution

$$\left(e^{eq}_{T_1} - e^{eq}_{T_2}\right)\frac{D(\omega,p)}{4\pi}V_g(\omega,p). \tag{38}$$

The number of new particles is given by integrating (38) over all frequencies and polarizations and by multiplying the result by π to account for the integration over the solid angle $\int_{\phi=0}^{2\pi}\int_{\theta=0}^{\pi/2}\cos\theta\sin\theta d\theta d\phi$. The traveling direction of these particles is randomized on the half sphere pointing into the domain, and in the case of the hot boundary they are sent traveling to the right with a positive sign. Taking their mirror image, negative particles with the same properties are emitted by the cold boundary.

IV. VALIDATION

A. A ballistic problem

In order to validate the proposed formulation, we first consider a one-dimensional system bounded by two isothermal (Sec. III E 2) boundaries that are sufficiently close—their distance apart, L, is much smaller than all phonon mean free paths—that transport can be modeled as ballistic. The system is initially at a uniform equilibrium temperature T_0, when at $t = 0^+$ the temperature of the isothermal walls impulsively changes to $T_0 \pm \Delta T$.

Appendix B presents an analytical solution for the resulting transient evolution of the temperature field that is used here for comparison with our simulations. A particularly interesting case is the Debye model which, when coupled with small temperature amplitudes, allows a linearization of the general relation (B4) to provide a fairly simple closed-form solution (B5). Figure 4 shows a comparison between this solution and the variance-reduced Monte Carlo result. The simulation was run with $T_{eq} = T_0$ and the phonon velocity was taken to be 12 360 m s^{-1}.[10] Excellent agreement is observed.

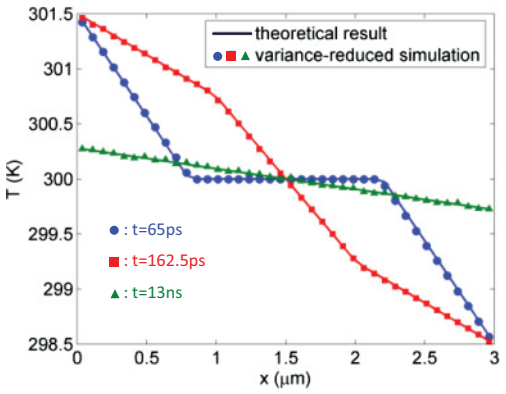

FIG. 4. (Color online) Transient temperature profile in a one-dimensional ballistic system whose boundary temperatures undergo an impulsive change at $t = 0$. Initially, the system is in equilibrium at temperature $T_0 = 300$ K. At $t = 0^+$, the wall temperatures become $T_0 \pm \Delta T$; here, $\Delta T = 3$ K.

B. Heat flux and thermal conductivity in a thin slab

In this section we continue to validate our formulation by calculating the thermal conductivity of a thin silicon slab bounded by two diffusely reflecting walls a distance d apart in the z direction (see Fig. 5). The slab is infinite in the x and y directions.

This problem is considered here because the solution can be expressed analytically. We introduce the local deviation function $f^d = f - f^{\rm loc}$ and, denoting the temperature gradient by dT/dy, rewrite the BTE at steady state as

$$V_g\frac{df^{\rm loc}}{dT}\frac{dT}{dy}\cos(\theta) + \mathbf{V}_g\nabla f^d = -\frac{f^d}{\tau}. \tag{39}$$

This equation can be solved to yield, in the coordinate system introduced in Fig. 5,

$$f^d(z,\omega,p,\theta,0<\phi<\pi) = -\Lambda(\omega,p,T_0)\cos(\theta)\frac{df^{\rm loc}(\omega,T_0)}{dT}\frac{dT}{dy}\left\{1-\exp\left[-\frac{z}{\Lambda(\omega,p,T_0)\sin(\theta)\sin(\phi)}\right]\right\}, \tag{40}$$

$$f^d(z,\omega,p,\theta,-\pi<\phi<0) = -\Lambda(\omega,p,T_0)\cos(\theta)\frac{df^{\rm loc}(\omega,T_0)}{dT}\frac{dT}{dy}\left\{1-\exp\left[-\frac{z-d}{\Lambda(\omega,p,T_0)\sin(\theta)\sin(\phi)}\right]\right\}, \tag{41}$$

where $\Lambda(\omega,p,T_0)$ is the average mean free path at frequency ω, polarization p, and temperature T_0, given by

$$\Lambda(\omega,p,T_0) = V_g(\omega,p)\tau(\omega,p,T_0). \tag{42}$$

Moments of this solution can be numerically integrated to yield values for the heat flux and the thermal conductivity of the slab.

In the simulation, we calculate the thermal conductivity by measuring the steady state heat flux in response to a temperature gradient along the y axis (see Fig. 6). Due to the translational symmetry of the system, we impose the temperature gradient using the periodic unit cell formulation presented in Sec. III E 3, which allows us to use a finite system size in the y direction, taken to be $L = 100$ nm. In order to measure the thermal conductivity at T_0, a temperature gradient is imposed by setting a target temperature of $T_0 + \Delta T$ for the hotter of the two boundaries and $T_0 - \Delta T$ for the colder boundary, and we proceed as explained in Sec. III E 3. The deviational method allows the solution of this problem

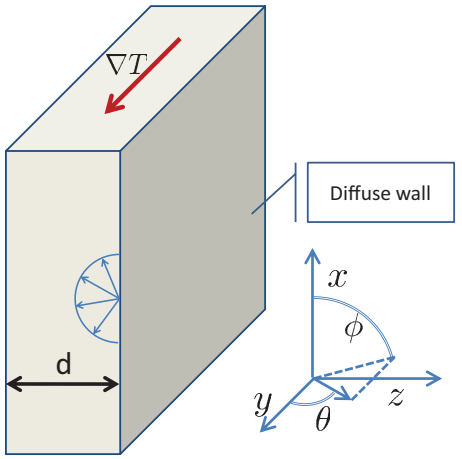

FIG. 5. (Color online) Heat conduction in a silicon slab due to an imposed temperature gradient in the y direction. Slab is infinite in the x and y directions.

for $\Delta T \ll T_0$ (here, $\Delta T = 0.05$ K), in contrast to non-variance-reduced methods that would require $\Delta T \sim T_0$ to achieve statistically significant results. The best choice for the equilibrium (control) temperature is clearly $T_{eq} = T_0 = 300$ K. Initialization of the simulation at equilibrium at T_0 is also convenient, because no particles need to be generated for the initial configuration.

Figure 7 compares the heat flux in the y direction inside a slab of silicon (see Appendix A for material parameters) of thickness $d = 100$ nm, as computed by the deviational method, to the analytical solution. Figure 8 compares the thermal conductivity of the slab at $T_0 = 300$ K as a function of d computed from the deviational method and from the analytical expression. Very good agreement is observed in all cases.

V. COMPUTATIONAL EFFICIENCY

The variance-reduced method developed here allows substantial improvement in the relative statistical uncertainty $\sigma/\Delta T$ compared to non-variance-reduced simulations. Here, σ is the standard deviation in the temperature measurement and ΔT is the characteristic temperature difference (as, for example, in the validation case studied in Sec. IV B).

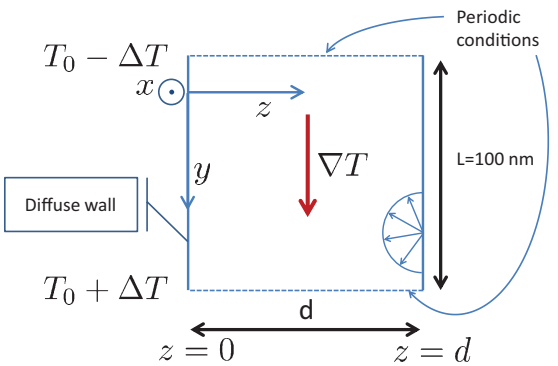

FIG. 6. (Color online) Simulation geometry. Boundaries at $z = 0$ and $z = d$ are diffusely reflecting. Infinite domain in the y direction is terminated by use of periodic boundaries $L = 100$ nm apart.

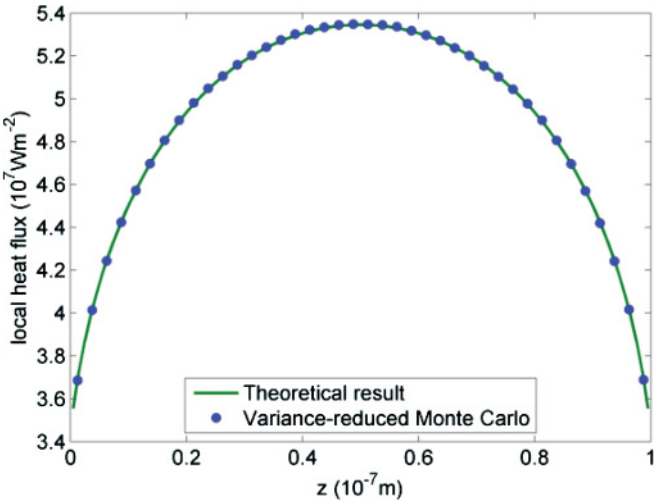

FIG. 7. (Color online) Spatial variation of the axial (in the y direction) heat flux in a thin film with a thickness $d = 100$ nm, computed theoretically and compared to the result of the deviational simulation.

Figure 9 compares the relative statistical uncertainty of the variance-reduced with the standard method. The reported data were obtained by simulating equilibrium at some temperature T_1 and defining $\Delta T = T_1 - T_0$ as the characteristic signal that needs to be resolved. By choosing $T_{eq} = T_0$ in the deviational method, we ensure that finite deviation from equilibrium is considered and thus the statistical uncertainty is nonzero. Simulation of an equilibrium state is a matter of convenience, because in nonequilibrium problems the number of particles and thus the local statistical uncertainty vary as a function of space in the deviational simulation and are thus difficult to quantify precisely; simulations of simple problems (e.g., Couette-type problems) in the past[5,12,13] have yielded very similar results. We also note that, even though this Figure compares relative statistical uncertainties, this information can

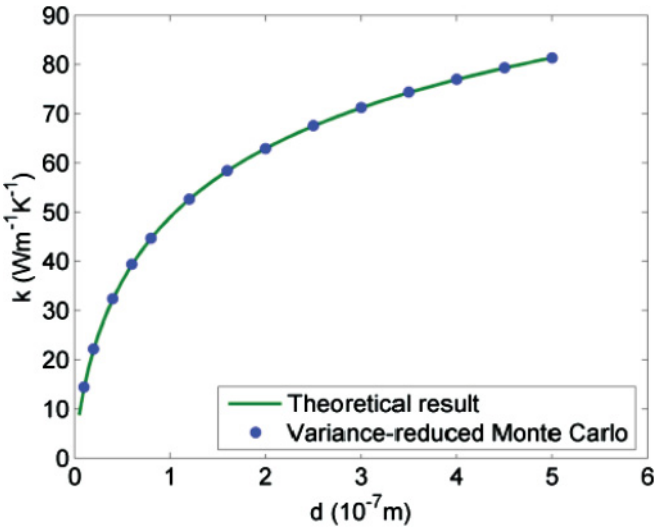

FIG. 8. (Color online) Theoretical values of the thin film thermal conductivity at $T_0 = 300$ K, computed by numerical integration of the theoretical expressions (40) and (41), and compared with the values obtained from the deviational simulation.

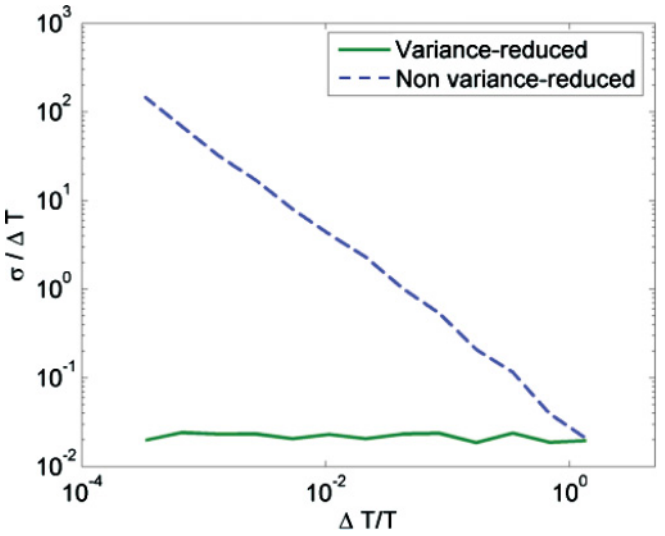

FIG. 9. (Color online) Comparison of relative statistical uncertainties for equilibrium systems at temperature T_1 with $\Delta T = T_1 - T_0$ and $T_0 = 300$ K.

be used to infer the computational speedup, because the cost of the deviational simulation per timestep is very similar to that of the standard Monte Carlo method. Specifically, the speedup provided by the deviational method is given by the square of the ratio of the relative statistical uncertainties.

A very interesting feature of variance-reduced methods is that the standard deviation of the results is proportional to the amplitude ΔT of the signal, as shown in Fig. 9 (see also Refs. 5, 22, and 23). As a consequence, variance-reduced methods are able to provide the desired relative statistical uncertainty (noise-to-signal ratio) for arbitrarily low signals without requiring more computational effort. In contrast, in the case of the non-variance-reduced methods, it is more computationally expensive to obtain the desired level of relative statistical uncertainty for small than for large variations in temperature. In these methods, for $\Delta T \ll T_0$, the statistical uncertainty is approximately constant (set by equilibrium fluctuations) and thus $\sigma/\Delta T \sim 1/\Delta T$. As a result, the speedup offered by the variance-reduced methods scales as $1/(\Delta T)^2$. For example, at $\Delta T/T_0 \approx 10^{-2}$ (i.e., $\Delta T \approx 3$ K at room temperature) the speedup is approximately four orders of magnitude (see Fig. 9); at $\Delta T/T_0 \approx 10^{-3}$, the speedup is approximately six orders of magnitude.

VI. APPLICATIONS

In this section we present some applications of the deviational method to problems of current engineering interest. Modeling work in these areas is still ongoing; the objective of this discussion is mainly to showcase the capabilities of the proposed method.

A. Thermal conductivity of nanoporous silicon: Influence of nanopore alignment

Decreasing the thermal conductivity as a means of improving the thermoelectric effect has received considerable attention, and nanostructures are a novel approach toward this goal. Similarly to Huang *et al.*[21] and Jeng *et al.*,[4] we assess here the thermal conductivity of nanostructured materials. The nanostructure considered here is made of rectangular pores as shown in Fig. 3. We model it as a 2D problem (possible if the material boundaries in the directions normal to the plane shown in the figure can be approximated as specularly reflecting). Figure 10 shows the periodic cell considered and defines the parameter d that we use to describe the spatial distribution of the pores. The thermal conductivity in the y direction is measured by imposing periodic unit cell boundary conditions as explained in Sec. III E 3, with a temperature difference of 0.1 K across the unit cell. Using the data of Appendix A, the contributions of the different mean free paths to the bulk thermal conductivity can be calculated.

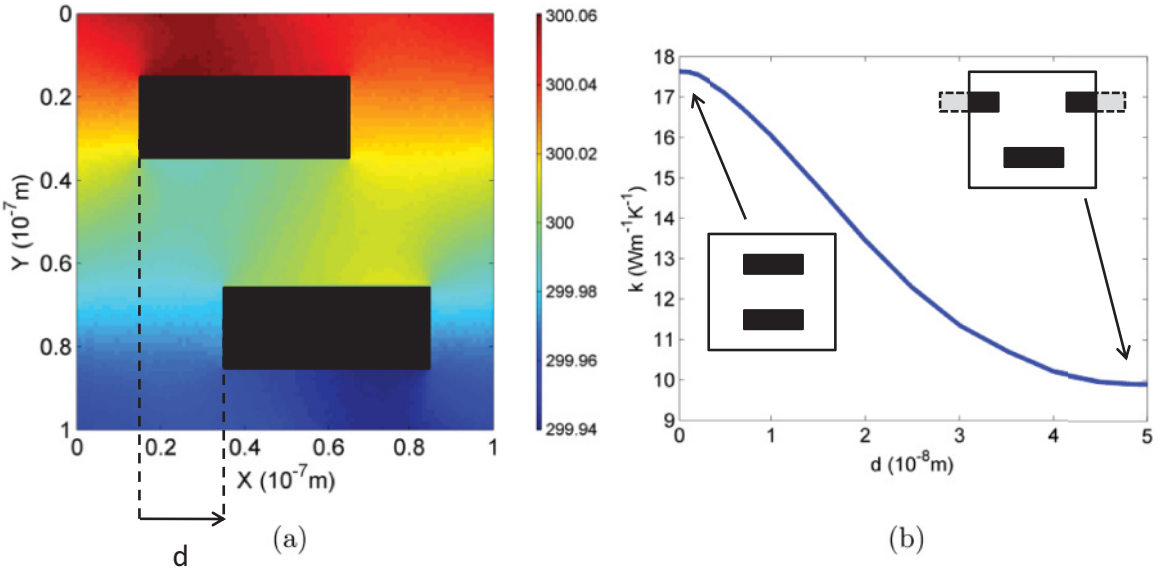

FIG. 10. (Color online) (a) Temperature field in a unit cell of a periodic nanoporous material. (b) Thermal conductivity as a function of parameter d.

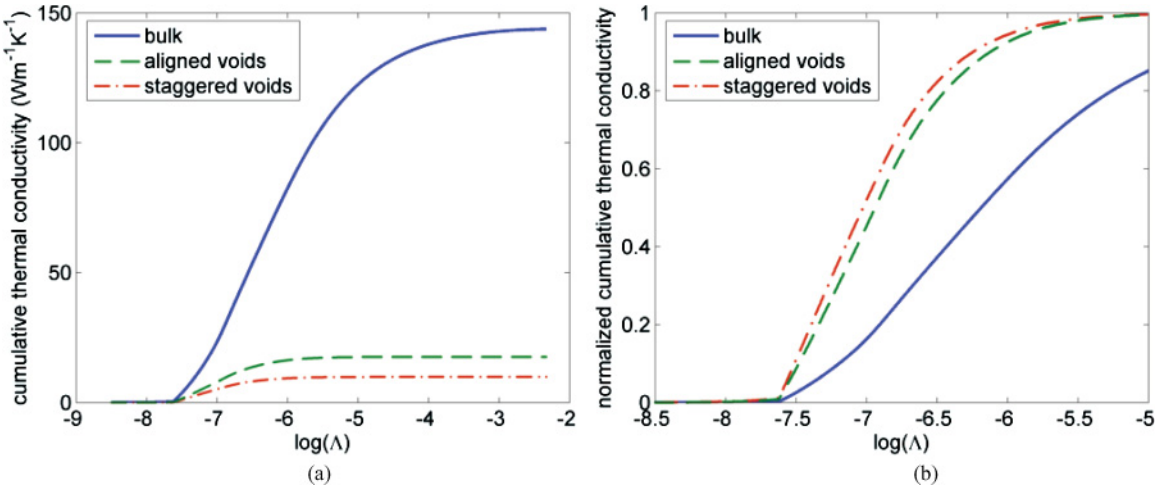

FIG. 11. (Color online) (a) Thermal conductivity accumulation as a function of the mean free path. The bulk conductivity was computed by numerical integration of the thermal conductivity per unit frequency, $\tau v^2 C_\omega/3$ (Refs. 15, 24, and 1); here, C_ω is the heat capacity per frequency unit. (b) Normalized thermal conductivity accumulation, highlighting the influence of ballistic effects on the thermal conductivity.

A plot of the effective thermal conductivity, as computed with the deviational variance-reduced method, is displayed in Fig. 10. The thermal conductivity is reduced by almost a factor of 2 because of this geometrical effect. This highlights the importance of ballistic effects.

The importance of ballistic effects is further highlighted by Fig. 11, which shows that at $T_0 = 300$ K, mean free paths from 50 nm to 10 μm contribute significantly to the thermal conductivity of the bulk material; the presence of voids with period of 100 nm affects the contribution of all mean free paths, but completely suppresses the contribution of all mean free paths greater than about 1 μm. Tuning of the alignment parameter decreases further the contribution of the mean free paths between 50 nm and 1 μm.

B. Simulation of thermal conductivity spectroscopy

Figure 12 depicts an experimental setup developed in the MIT Nanoengineering Laboratory[25] as a prototype "thermal conductivity spectroscopy" system. This experiment is based on pump-probe transient thermoreflectance, in which a pump pulse is used to change the physical properties of a sample and a probe pulse is used to measure the change. In this experiment, a thin film of aluminum (thickness between 50 and 100 nm) is deposited on a silicon wafer and is initially at uniform temperature, say 300 K. At $t = 0$, localized laser irradiation creates a hot spot, shown in Fig. 12 as centered on the origin ($r = 0, z = 0$) of the coordinate system. A reliable description of the subsequent evolution of the temperature field is central to interpreting the experimental results and creating a means for inferring phonon mean free paths (the goal of this experiment) from experimental measurements (e.g., of surface temperature).

Given the scale of the aluminum slab, the impulsive nature of the heating, and the short duration of the phenomenon, phonon ballistic behavior needs to be accounted for, necessitating a Boltzmann treatment. However, this problem is very difficult (if not impossible) to simulate using standard Monte Carlo methods: the initial perturbation to the temperature field is small in amplitude (see below), which makes resolution of transient results very costly. Moreover, the need to simulate early as well as late times and avoid artifacts from artificial domain termination makes the simulation of a large computational domain necessary, even though the original hot spot is very small. In traditional Monte Carlo methods, this large computational domain would need to be filled with particles.

The method proposed makes this calculation possible. Simulation of the deviation from equilibrium allows the calculation to proceed using zero particles in regions not yet affected by the heating pulse. Thus, in addition to variance reduction, which removes the limitations associated with statistical uncertainty, simulation of the deviation from equilibrium simultaneously considerably reduces the computational cost resulting from

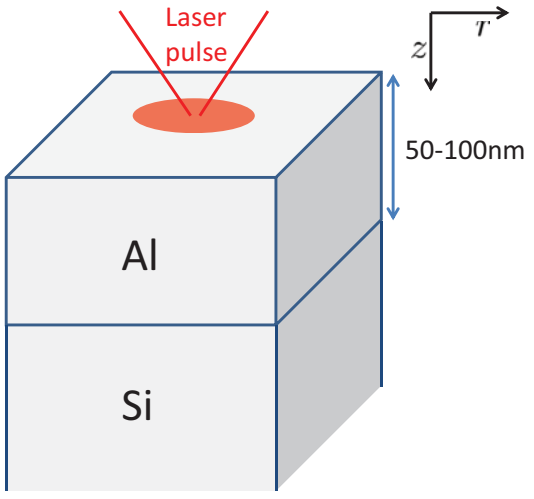

FIG. 12. (Color online) System composed of a slab of aluminum on a semi-infinite silicon wafer, used for transient thermoreflectance experiments. At $t = 0$, a laser pulse induces a temperature field $T(r,z,t)$. The temperature field evolution after the pulse is computed by assuming that the aluminum surface is adiabatic.

the multiscale nature of this problem. We also note that, by taking the equilibrium distribution at 300 K, the simulation only has positive particles. Hence there will be no cancellation of particles, and the entire simulation will run with a fixed amount of particles.

In practice, one can exploit the cylindrical symmetry in order to reduce the problem dimensionality: the resulting temperature field is expected to depend only on the depth z and on the distance from the center of the pulse, r. Therefore, we can use toroidal cells to sample the temperature and process the scattering. The only drawback is that cells near the center, at small radius, will have a smaller volume and will sample the temperature over a smaller number of particles, thus yielding noisier results in these regions.

1. Initial condition

As stated above, since the material is originally at equilibrium at $T_0 = 300$ K, it is most convenient, but also computationally efficient, to choose $T_{eq} = T_0$. Laser irradiation introduces a heating effect in a thin layer close to the irradiated surface, which has been parametrized[15] using the expression

$$\Delta T(r,z) = T - T_0 = A \exp\left(-\frac{2r^2}{R_0^2} - \beta z\right) \tag{43}$$

with $A = 1$ K, $R_0 = 15$ μm, and $\beta^{-1} = 7$ nm. This expression is used here as an initial condition for the material temperature. Regions for which $\Delta T < 0.005$ K were taken to be at equilibrium at $T_0 = T_{eq}$ (no particles).

2. Interface modeling

The top surface of the aluminum material ($z = 0$) is modeled as a diffusely reflecting wall.

Modeling of the interface between the two materials accurately is still an active area of research. Here, we chose to use a recently developed model[15,26] which relates the transmissivity to the interface conductance G through the expression

$$\langle P_{1\to 2} C_1 V_{g,1}\rangle = \frac{2}{\frac{1}{\langle C_1 V_{g,1}\rangle} + \frac{1}{\langle C_2 V_{g,2}\rangle} + \frac{1}{2G}}. \tag{44}$$

Here, $P_{i\to j}$ denotes the probability for a phonon to pass through the interface from material i to j; the angular brackets denote integration over frequency and sums over polarization, while C_1 and C_2 denote the volume heat capacity per unit frequency in media 1 and 2, respectively. In this model, we assume that the interface is totally diffuse: the direction of an incident particle is reset regardless of the transmission or reflection of the particle, while its frequency and polarization are retained.[27] For the interface conductance G, we use the experimental value $G = 1.1 \times 10^8$ W m^{-2} K^{-1}.[26]

We also utilize the expression[27]

$$\begin{aligned} &D_1(\omega,p) V_{1,g}(\omega,p) f_{T_0}^{eq} P_{1\to 2}(\omega,p) \\ &\quad = D_2(\omega,p) V_{2,g}(\omega,p) f_{T_0}^{eq} P_{2\to 1}(\omega,p), \end{aligned} \tag{45}$$

which relates the probability for a phonon with radial frequency ω and polarization p to pass through the interface from 1 to 2 to the probability to pass from 2 to 1.

We can easily verify that relation (45) applies when the deviational energy e^d is used instead of the phonon distribution. Additionally, expression (44) which relies on, among other things, (45),[15,26] also remains unchanged when applied to deviational particles.

Following Refs. 15 and 26, we let $P_{1\to 2}$ be a constant [which makes it easy to calculate from (44)] and deduce $P_{2\to 1}$ from (45). In our case we chose to set $P_{\mathrm{Al}\to\mathrm{Si}}$ constant, except for the high-frequency transverse acoustic modes; since the cutoff frequency of the TA branch in Si is lower than the TA cutoff frequency in Al, phonons with such frequencies must undergo total reflection.[15] Similarly, LA phonons in Si whose frequency is above the aluminum LA branch cutoff frequency are totally reflected.

3. Domain termination

At long times, phonons may travel far from the hot spot. In order to avoid discretizing an infinite domain with computational cells (for calculating the temperature), we restrict our discretization to a finite (but large) "nominal" domain. In order to simulate the actual system accurately and consistently, we keep track of the particles even after they have left the nominal part of the domain.

Particles that leave this domain are not sampled (for calculating the temperature and pseudotemperature), but are still scattered by assuming a local temperature of 300 K as an input parameter for the relaxation time. This amounts to a linearization of the collision operator at $T = 300$ K and is based on the reasonable assumption that, sufficiently far from the heating source, the temperature is very close to 300 K. Particles that leave the nominal part of the domain may reenter it, hence ensuring a rigorous treatment of the semi-infinite region.

Particular care is taken to ensure that the frequency and polarization of a particle is drawn from the correct distribution, because energy conservation—built into the simulation method—requires that the number of particles is conserved by the scattering process and is inconsistent with approximations which do not conserve energy. For example, setting $T_{\mathrm{loc}} = 300$ K is inconsistent with energy conservation because $e^{\mathrm{loc}}(T_{\mathrm{loc}} = 300\ \mathrm{K}) - e^{eq} = 0$, which implies no particle generation, which in the presence of particle deletion due to the term $-e^d/\tau$ leads to net particle and thus energy loss. This situation can be rectified by allowing the temperature at the particle position to be different from T_{eq}; specifically, we write $T = T_{eq} + \epsilon$ and expand

$$\frac{D(\omega,p)\left(e^{\mathrm{loc}} - e^{eq}_{T_{eq}}\right)}{\tau(\omega,p,T_{eq})} \approx \frac{D(\omega,p)}{\tau(\omega,p,T_{eq})} \frac{\partial e^{eq}_{T_{eq}}}{\partial T}\epsilon. \tag{46}$$

Frequencies and polarizations are thus drawn from

$$\frac{D(\omega,p)}{\tau(\omega,p,T_{eq})} \frac{\partial e^{eq}_{T_{eq}}}{\partial T}, \tag{47}$$

since (46), once normalized, does not depend on the local ϵ. As before, energy conservation is ensured by simply conserving the particles.

In addition to providing a method for terminating simulations, this approach represents a promising avenue for treating the entire simulation domain in the limit that linearization of

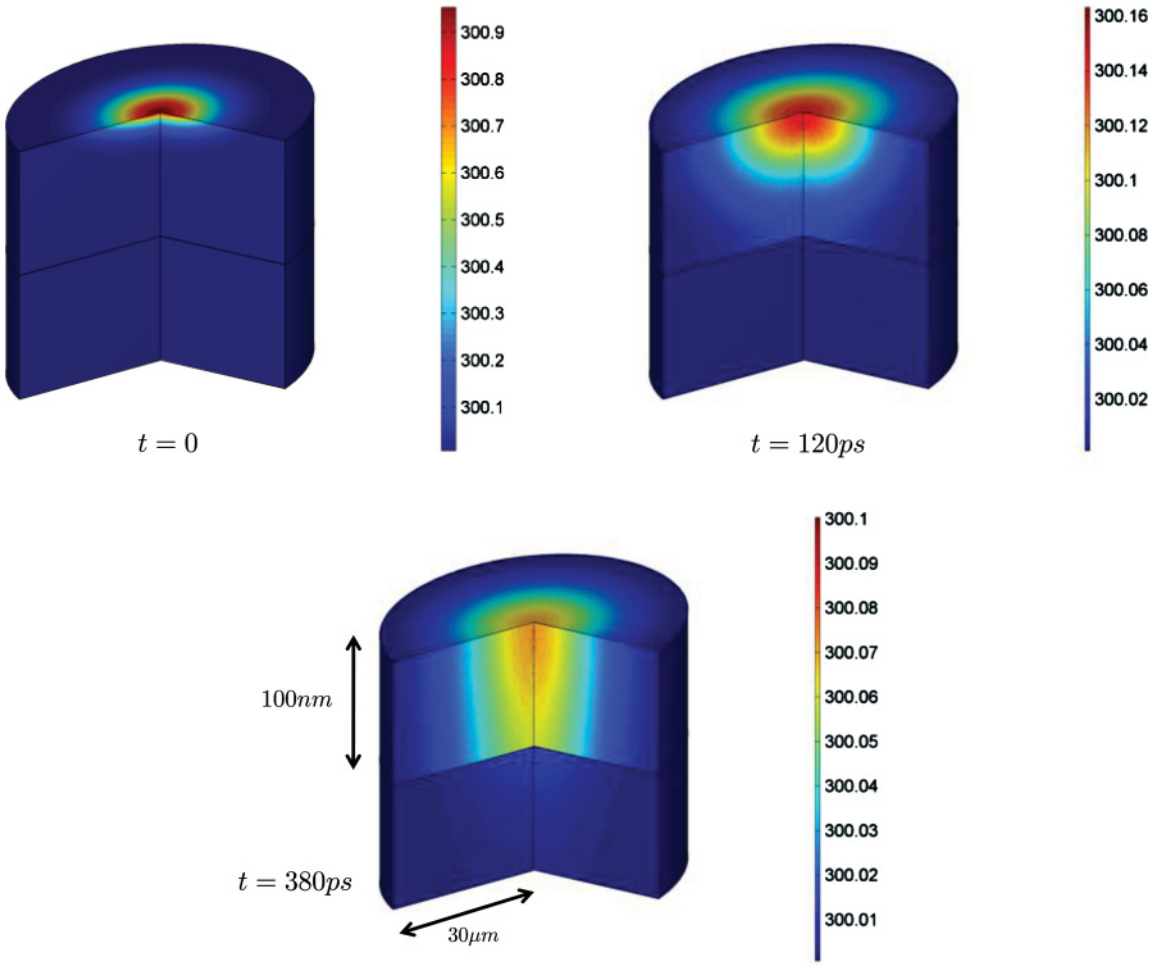

FIG. 13. (Color online) Variance-reduced temperature field in an aluminum slab and supporting silicon wafer after initial heating by a laser pulse. The picture shows the aluminum slab (100 nm thickness) and a portion of the silicon wafer (100 nm thickness).

the collision operator is appropriate. The advantage of this formulation is a significant reduction in computational cost because evaluation of the local temperature and pseudotemperature is not required at every time step. Further details will be given in a future publication.

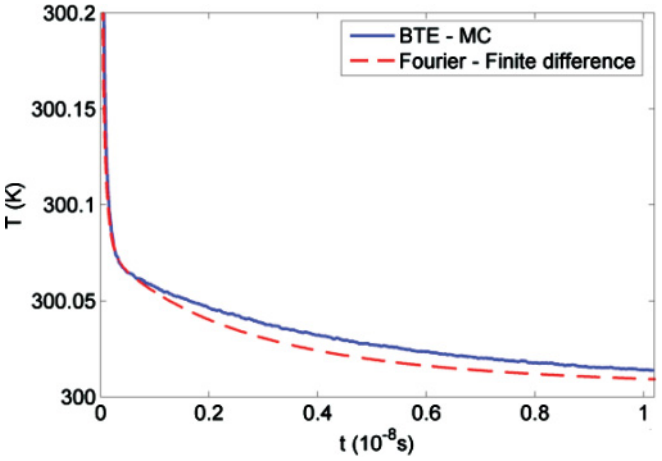

FIG. 14. (Color online) Surface temperature at the hot spot (averaged over the region $0 \leqslant r \leqslant 2\ \mu$m, $0 \leqslant z \leqslant 5$ nm) as a function of time after initial heating by laser pulse. The difference from the solution based on the Fourier model is a result of ballistic effects.

4. Simulation results

Figures 13 and 14 show that the variance-reduced method developed here can calculate the temperature field with small statistical uncertainty. This is remarkable given the minute temperature differences [$O(0.01)$ K] present in this problem, especially at late times. For such temperatures, according to Fig. 9, the speedup compared to a standard Monte Carlo method is on the order of 10^9.

Figure 14 compares our simulation results with a numerical solution of the heat conduction equation (Fourier's law). The differences between the two predictions are a result of nondiffusive (ballistic or transitional) effects. The detailed information available in simulations of this phenomenon can assist in the development of methodologies for characterizing carrier mean free paths from comparisons such as the one shown in Fig. 14. Here, we note that the present calculation does not account for thermal transport by electrons in aluminum. This was neglected in the interest of simplicity and because the primary focus of this experiment is transport

through the silicon substrate.[15] Thermal transport by electrons in aluminum will be considered and evaluated in a future publication.

VII. DISCUSSION

We have shown that efficient and accurate algorithms for solving the BTE with significantly reduced statistical uncertainty can be developed by focusing on the deviation from a nearby equilibrium within an energy-based formulation. The energy-based formulation facilitates exact energy conservation, thus improving the simulation fidelity, while the variance reduction is made possible by the deterministic information inherent in the Bose-Einstein distribution which describes the nearby equilibrium. The proposed method was validated using analytical solutions of the Boltzmann transport equation. Very good agreement with the analytical results was found.

The proposed algorithm was used to study the effect of porosity on the effective thermal conductivity of pure silicon. Our results show that the staggering of periodically arranged voids at small scales exploits ballistic shading to effect reduction in the effective thermal conductivity. A more systematic investigation of the effects of porosity on the effective conductivity of silicon—including anisotropic effects—will be the subject of future work.

We also presented simulations of a recently developed experimental technique known as thermal conductivity spectroscopy, in which the transient response of a thin aluminum slab over a silicon wafer to a localized heating induced by a laser pulse is used to infer properties of heat carriers. These simulations required the development of a domain termination algorithm for rigorously treating deviational particles as they travel to regions far from the heating source, without having to sample these particles everywhere in this semi-infinite region. This latter algorithm corresponds to a linearization of the collision operator and may, in fact, form the basis of a significantly more efficient simulation approach valid in cases where linearization is appropriate.

In addition to illustrating the benefits of variance reduction, simulations of the thermal conductivity spectroscopy problem also showcase the value of the proposed simulation approach as a multiscale method: in contrast to typical multiscale methods which focus on spatial decomposition of the domain into the particle and continuum subdomains, the present algorithm achieves a seamless transition from one description to the other by instead *algebraically* decomposing the distribution function into a part described by particles and a part described deterministically.[28] Although here the simplest such implementation has been presented [a deterministic description in equilibrium at temperature $T_0 \neq T_0(\mathbf{x},t)$], deviational algorithms featuring a deterministic description that varies as a function of space [$e^{eq} = e^{eq}(\mathbf{x})$] have been developed[12,13] and shown to achieve improved variance reduction as $Kn \to 0$,[13] albeit at the cost of a moderately more complex algorithm. In the problem considered here, the continuum behavior at large distances from the heat source is in fact equilibrium at T_0 and thus the present algorithm is sufficient. However, in other problems where a local equilibrium is present in large parts of the domain, algebraic decomposition using $e^{eq} = e^{eq}(\mathbf{x})$ will be able to provide considerable computational savings by considerably reducing the number of particles required for its simulation.

ACKNOWLEDGMENTS

The authors are indebted to Colin Landon, Gregg Radtke, and Austin Minnich for many useful comments and discussions. This work was supported in part by the Singapore-MIT Alliance. J-P.M.P. gratefully acknowledges financial support from Ecole Nationale des Ponts et Chaussées and the MIT Department of Materials Science and Engineering through a Graduate Fellowship.

APPENDIX A: NUMERICAL DATA FOR SCATTERING RATES

In the simulations presented here we use data for the dispersion relations and for the relaxation times of phonons in Al and Si. Dispersion relations are adapted from experimental measurements in the [100] direction (from Ref. 29 for Al, and from Refs. 30 and 15 for Si).

For Al, as in Refs. 26 and 15 we assume a constant relaxation time chosen to match the desired lattice thermal conductivity. We therefore take

$$\tau_{\mathrm{Al}} = 10^{-11}\ \mathrm{s} \tag{A1}$$

For Si, we use the expressions from Refs. 15,31, with constants from Ref. 15. Relaxation times for acoustic modes are as follows:

$$\text{Phonon-phonon scattering,} \quad \text{LA}$$
$$\tau_L^{-1} = A_L \omega^2 T^{1.49} \exp\left(\frac{-\theta}{T}\right)$$

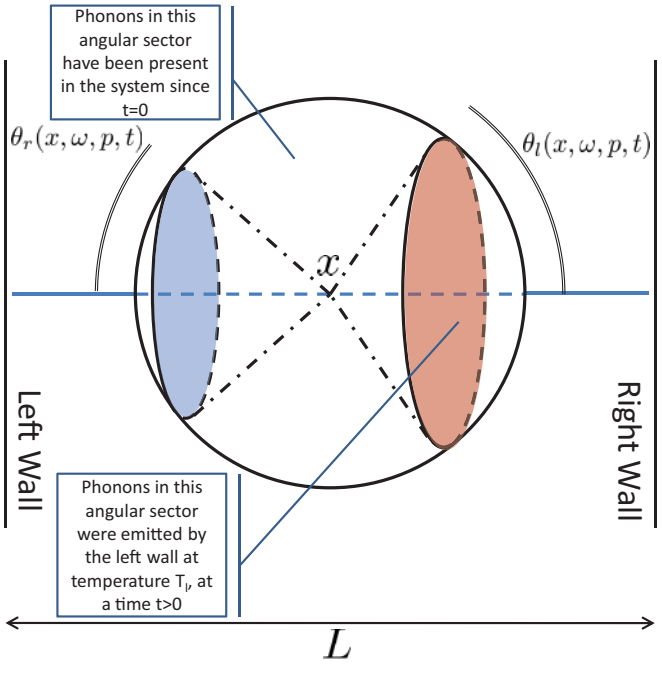

FIG. 15. (Color online) At a given point in space, the solid angle can be divided into three distinct regions in which the distribution of phonons is known; here, θ_l is given by $\cos(\theta_l) = x/[V_g(\omega,p)t]$, while θ_r is given by $\cos(\theta_r) = (L-x)/[V_g(\omega,p)t]$.

Phonon-phonon scattering, TA

$$\tau_T^{-1} = A_T \omega^2 T^{1.65} \exp\left(\frac{-\theta}{T}\right)$$

Impurity scattering $\tau_I^{-1} = A_I \omega^4$

Boundary scattering $\tau_B^{-1} = w_b$

where the constants take the following values:

Parameter	A_L	A_T	θ	A_I	w_b
Value (in SI units)	2×10^{-19}	1.2×10^{-19}	80	3×10^{-45}	1.2×10^{6}

The total relaxation time for a given polarization is obtained using the Matthiessen rule

$$\tau^{-1} = \sum_i \tau_i^{-1}. \tag{A2}$$

Optical phonons in Si are considered immobile (Einstein model). Einstein's model states that the contribution of optical phonons to the vibrational energy per unit volume in a crystal is given by[1]

$$U = \frac{N_p N' \hbar \omega_E}{V[\exp(\hbar\omega_E/k_b T) - 1]}, \tag{A3}$$

where $N_p = 3$ is the number of polarizations, $N' = 1$ is the number of optical states per lattice point, ω_E is the Einstein radial frequency [$\omega_E = 9.1 \times 10^{13}$ s^{-1} (Refs. 30 and 15)], and V is the volume of a lattice point (with a lattice constant $a = 5.43$ Å, $V = a^3/4 = 4 \times 10^{-29}$ m^3).

For the relaxation time of optical phonons, we use the value[32]

$$\tau_O = 3 \times 10^{-12} \text{ s}. \tag{A4}$$

APPENDIX B: DERIVATION OF THE TRANSIENT BALLISTIC 1D SOLUTION

Following the impulsive change of temperature at the walls from T_0 to $T_l = T_0 + \Delta T$ and $T_r = T_0 - \Delta T$, thermalized phonons at temperature T_r and T_l are emitted from the "right" and "left" walls, respectively (see Fig. 15). For some arbitrary location x, for a given frequency, polarization, and time, the angular space can be divided into three distinct domains characterized by two angles $\theta_r(x,\omega,p,t)$ and $\theta_l(x,\omega,p,t)$, as depicted in Fig. 15. Phonons described by $0 < \theta < \theta_l$ were emitted by the left wall at a time $t > 0$. Phonons described by $\theta_l < \theta < \pi - \theta_r$ have been present in the system since $t = 0$. Phonons described by $\pi - \theta_r < \theta < \pi$ were emitted by the right wall at a time $t > 0$.

The energy can therefore be written as

$$\begin{aligned} E_V(x,t) = \frac{1}{2}\sum_p \Bigg\{ & \int_\omega \int_{\theta=0}^{\theta_l(x,\omega,p,t)} e_{T_l}^{eq}(\omega) D(\omega,p) \sin(\theta) d\theta d\omega \\ & + \int_\omega \int_{\theta=\theta_l(x,\omega,p,t)}^{\pi-\theta_r(x,\omega,p,t)} e_{T_0}^{eq}(\omega) D(\omega,p) \sin(\theta) d\theta d\omega \\ & + \int_\omega \int_{\theta=\pi-\theta_r(x,\omega,p,t)}^{\pi} e_{T_r}^{eq}(\omega) D(\omega,p) \sin(\theta) d\theta d\omega \Bigg\}. \end{aligned} \tag{B1}$$

From geometrical considerations,

$$\cos[\theta_r(x,\omega,p,t)] = \min\left(1, \frac{L-x}{V_g(\omega,p)t}\right) = 1 - \left(1 - \frac{L-x}{V_g(\omega,p)t}\right) H\left(1 - \frac{L-x}{V_g(\omega,p)t}\right), \tag{B2}$$

$$\cos[\theta_l(x,\omega,p,t)] = \min\left(1, \frac{x}{V_g(\omega,p)t}\right) = 1 - \left(1 - \frac{x}{V_g(\omega,p)t}\right) H\left(1 - \frac{x}{V_g(\omega,p)t}\right), \tag{B3}$$

where H is the Heaviside function. Proceeding to the integration in θ, the energy density is given by

$$\begin{aligned} E_V(x,t) = \frac{1}{2}\sum_p \Bigg\{ & \int_\omega \left(1 - \frac{x}{V_g(\omega,p)t}\right) H\left(1 - \frac{x}{V_g(\omega,p)t}\right) e_{T_l}^{eq}(\omega) D(\omega,p) d\omega \\ & + \int_\omega \left(1 - \frac{L-x}{V_g(\omega,p)t}\right) H\left(1 - \frac{L-x}{V_g(\omega,p)t}\right) e_{T_r}^{eq}(\omega) D(\omega,p) d\omega \\ & + \int_\omega \left[1 - \left(1 - \frac{x}{V_g(\omega,p)t}\right) H\left(1 - \frac{x}{V_g(\omega,p)t}\right)\right] e_{T_0}^{eq}(\omega) D(\omega,p) d\omega \\ & + \int_\omega \left[1 - \left(1 - \frac{L-x}{V_g(\omega,p)t}\right) H\left(1 - \frac{L-x}{V_g(\omega,p)t}\right)\right] e_{T_0}^{eq}(\omega) D(\omega,p) d\omega \Bigg\}. \end{aligned} \tag{B4}$$

The temperature $T = T(x,t)$ is obtained by numerically finding the Bose-Einstein distribution corresponding to this energy density.

Using the Debye model and considering small temperature changes ($|T_r - T_0| \ll T_0$ and $|T_l - T_0| \ll T_0$), we can express the resulting temperature field in a simpler form. The first assumption allows the removal of the frequency and polarization dependence on the group velocity, while the second assumption allows the linearization of the Bose-Einstein terms in the integrals. Several simplifications can then be carried out to yield the following expression for the temperature field:

$$\Delta T(x,t) = \frac{1}{2}\left(1 - \frac{x}{V_g t}\right) H\left(1 - \frac{x}{V_g t}\right) \Delta T_l + \frac{1}{2}\left(1 - \frac{L-x}{V_g t}\right) H\left(1 - \frac{L-x}{V_g t}\right) \Delta T_r . \tag{B5}$$

[1] G. Chen, *Nanoscale Energy Transport and Conversion* (Oxford University Press, New York, 2005).
[2] A. Majumdar, J. Heat Transfer **115**, 7 (1993).
[3] G. Chen, M. S. Dresselhaus, G. Dresselhaus, J.-P. Fleurial, and T. Caillat, Int. Mater. Rev. **48**, 45 (2003).
[4] M.-S. Jeng, R. Yang, D. Song, and G. Chen, J. Heat Transfer **130**, 042410 (2008).
[5] L. L. Baker and N. G. Hadjiconstantinou, Phys. Fluids **17**, 1 (2005).
[6] G. A. Bird, *Molecular Gas Dynamics and the Direct Simulation of Gas Flows* (Clarendon Press, Oxford, 1994).
[7] R. B. Peterson, J. Heat Transfer **116**, 815 (1994).
[8] S. Mazumder and A. Majumdar, J. Heat Transfer **123**, 749 (2001).
[9] D. Lacroix, K. Joulain, and D. Lemonnier, Phys. Rev. B **72**, 064305 (2005).
[10] Q. Hao, G. Chen, and M.-S. Jeng, J. Appl. Phys. **106**, 114321 (2009).
[11] T. M. M. Homolle and N. G. Hadjiconstantinou, Phys. Fluids **19**, 041701 (2007).
[12] T. M. M. Homolle and N. G. Hadjiconstantinou, J. Comput. Phys. **226**, 2341 (2007).
[13] G. A. Radtke and N. G. Hadjiconstantinou, Phys. Rev. E **79**, 056711 (2009).
[14] G. A. Radtke, N. G. Hadjiconstantinou, and W. Wagner, Phys. Fluids **23**, 030606 (2011).
[15] A. J. Minnich, Ph.D. thesis, Massachusetts Institute of Technology, 2011.
[16] Y. K. Koh and D. G. Cahill, Phys. Rev. B **76**, 075207 (2007).
[17] P. G. Klemens, Solid State Phys. **7**, 1 (1958).
[18] A. Mittal and S. Mazumder, J. Heat Transfer **132**, 052402 (2010).
[19] G. A. Radtke, Ph.D. thesis, Massachusetts Institute of Technology, 2011.
[20] D. Lacroix, K. Joulain, D. Terris, and D. Lemonnier, Appl. Phys. Lett. **89**, 103104 (2006).
[21] M.-J. Huang, T.-C. Tsai, L.-C. Liu, M.-S. Jeng, and C.-C. Yang, Comput. Model. Eng. Sci. **42**, 107 (2009).
[22] N. G. Hadjiconstantinou, Phys. Fluids **18**, 111301 (2006).
[23] N. G. Hadjiconstantinou, G. A. Radtke, and L. L. Baker, J. Heat Transfer **132**, 112401 (2010).
[24] J.-P. M. Péraud, M.S. thesis, Massachusetts Institute of Technology, 2011.
[25] A. J. Minnich, J. A. Johnson, A. J. Schmidt, K. Esfarjani, M. S. Dresselhaus, K. A. Nelson, and G. Chen, Phys. Rev. Lett. **107**, 095901 (2011).
[26] A. J. Minnich, G. Chen, S. Mansoor, and B. S. Yilbas (unpublished).
[27] G. Chen, Phys. Rev. B **57**, 14958 (1998).
[28] G. A. Radtke, J.-P. M. Péraud, and N. G. Hadjiconstantinou (accepted for publication).
[29] R. Stedman and G. Nilsson, Phys. Rev. **145**, 492 (1966).
[30] [http://www.ioffe.ru/SVA/NSM/Semicond/Si/mechanic.html].
[31] A. S. Henry and G. Chen, J. Comput. Theor. Nanosci. **5**, 141 (2008).
[32] P. G. Klemens, Phys. Rev. **148**, 845 (1966).